IJE TRANSACTIONS A: Basics Vol. 25, No. 3, (July 2012) 249-264

International Journal of Engineering

Journal Homepage: www.ije.ir

Nonlinear Analysis of a Flexible Beam Actuated by a Couple of Active SMA Wire Actuators

H. Sayyaadi*, M. R. Zakerzadeh

School of Mechanical Engineering, Sharif University of Technology, Tehran , P.O. Box 11155-9567, Iran

ARTICLE INFO

Article history:
Received 06 June2010
Received in revised form 03 September 2012
Accepted 19 April 2012

Keywords:
Nonlinear Modeling
Flexible Beam
SMA Actuators

ABSTRACT

There are two different ways of using SMA wires as actuators for shape control of flexible structures; which can be either embedded within the composite laminate or externally attached to the structure. Since the actuator can be placed at different offset distances from the beam, external actuators produce more bending moment and, consequently, considerable shape changes with the same magnitude of the actuation force comparing to the embedded type. Such a configuration also provides fast convection which is very important in shape control applications that require a high-frequency response of SMA actuators.
Although combination and modeling of externally-attached SMA actuator wires and strips have been considered by many researchers, these studies have some weaknesses neglecting them yields a number of errors between theoretical and experimental results. In this work, the aforementioned limitations of attaching actuators to the smart structures have been removed and a flexible beam actuated by two active SMA actuators is nonlinearly modeled. The Brinson constitutive equations and thermoelectric equations for SMA materials are coupled with the nonlinear beam behavior and the coupled system of equations is numerically solved for some particular practical cases. The analysis method done in this paper can be easily extended to the complicated smart structure with externally-attached SMA wires.

doi: *10.5829/idosi.ije.2012.25.03a.07*

1. INTRODUCTION

Smart materials have been extensively used in recent years for their great potentials to revolutionize engineering applications and design, particularly for active and passive control of structures. Among these materials, shape memory alloys (SMAs) have been receiving more attention and study due to their ability to develop extremely large recoverable strains, as well as great force. SMAs are applied in a wide variety of fields such as aerospace, medical, civil and mechanical engineering [1].

Having adaptive structure is another characteristic for these SMA materials that has largely been considered in vibration control rather than shape control. One way of using SMA as actuator in these flexible structures is embedding or bonding it to the surface of the host material so that the moment of the actuating force deforms the structure. Although increasing the distance between the bonded actuator and the neutral axis of the structure enhances the moment, as a linear function, the flexural stiffness of the structure increases as a square of this distance [2]. Another difficulty of using SMA actuator in embedding form is its heat transfer. This problem constrains the high frequency response of SMA actuator which is very important in shape control applications where fast structure response is needed.

To overcome the limitations of bonded or embedded SMA actuators in structures, they can be externally attached to the structure. This configuration can be advantageous in several aspects. First, the actuators can be placed at different offset distances from the neutral axis of the structure and; consequently, produce more bending moment and shape change with the same magnitude of the actuation force (with respect to the embedded type) [3]. In addition, the increase in the flexural stiffness of the structure can be condoned. Such a configuration, also, eliminates the heat transfer problem mentioned before for embedding SMA within composite laminate.

Due to the fact that beams play an important role in structural mechanics, some researchers have paid

*Corresponding Author Email: *Sayyaadi@Sharif.edu* (H. Sayyaadi)

particular attention to the combination of flexible beams with SMA wires and strips. Chaudhry and Rogers [2], for example, considered the bending of beam under external attachment of SMA wire and demonstrated the possibility of using this configuration for shape control applications. The weakness of this research is that the actuation force of the SMA wire was not derived from the constitutive equations and a fixed value of an attached load was used. In addition, in order to solve the derived equations and get a closed form solution, they made use of linear Euler–Bernoulli beam assumption. Therefore, the region in which these results were valid was limited and could not be extended to large deflection cases. It is shown in that paper by increasing the number of points on the beam through which the actuator passes, the actuation force for getting a specified tip deflection soars accordingly. However, in these configurations the beam behavior is less nonlinear; consequently, the tip deflection or shape control turns out to be easier. Increasing the number of points on the beam through which one SMA actuator passes, as well as increasing the number of the actuators, therefore, is a great advantage for control applications. Likewise, Shu et al. [3] developed a thermomechanical model to predict the structural response of a flexible beam actuated with externally SMA wire actuators. They first carried out a geometrically nonlinear static analysis to investigate the deformed shape of a flexible cantilever beam caused by an externally-attached SMA wire actuated electrically. In that paper a one-dimensional simplification of the 3D model developed by Boyd and Lagoudas [4] was used for predicting the thermomechanical response of the attached SMA actuator. The actuation force applied by the SMA actuator to the beam was evaluated by solving a coupled problem combining a thermodynamic constitutive model of SMAs with the heat conduction equation in the SMA and the structural model of the beam. Despite the fact that two SMA wires –one active and another inactive- were attached to the Shu's experimental beam set-up, they did not take into account the coupling effect of the inactive wire with the beam structure, nor did they take into account the effect of the beam section twist.

Similar work was carried out by Brinson et al. [5]. The case studied by them was a cantilever beam with externally-attached SMA wire. The work took advantage of Brinson's constitutive law for thermomechanical behavior of SMAs and then coupled it with linear and nonlinear behavior of the controlled beam. In spite of the fact that they considered the effects imposed by the nonlinear terms, the connection point of the SMA wire to the base was selected at the root of the beam and this limited the mentioned results especially for the practical case where this point can be at any position. In addition, only one SMA wire was chosen for the actuation of the beam and the compound effect of the SMA heat transfer equation with the model was ignored. Moallem et al. [6], on the other hand, proposed a nonlinear control scheme for deflection control of a flexible beam system using shape memory alloy wires. Taking the equation of linear Euler–Bernouli beam and thermal characteristics of SMA wire into account, they developed a control scheme in order to regulate the force exerted by an SMA actuator attached to a flexible beam. Although two SMA wires -one active and another inactive- in a diagnostic configuration were used, they neglected the effect of inactive wire in the system of equations. Elsewhere, Sohn [7] investigated the control performance of a flexible beam structure by adopting SMA actuator with robust control algorithm. Here, an antagonistic type of actuator using two SMA wires is installed to a flexible beam structure. The governing equation of motion of the proposed flexible structure is obtained via Hamilton's principle by considering the linear Bernoulli-Euler beam. In addition, the dynamic characteristics of the SMA wire actuator are experimentally identified and incorporated with the governing equation. Although the proposed model has the inadequacies of the aforesaid research, it is sufficient and accurate for vibration control, where the structure is in small deflection mode.

In the present research, the above limitations of attaching SMA actuators to the smart structures have been resolved and nonlinear modeling of a flexible beam actuated by two active SMA actuators is carried out. In the first section of this paper, nonlinear formulation for a flexible beam, under two applied forces, is derived. One of these forces is applied at the tip of the beam and the other in the middle. To consider the generality of the modeling, the connection point of the SMA wires to the base is selected at any position in a plane.

In the second section, the Brinson thermomechanical constitutive equation of SMA wires is reviewed due to its simplicity and its applicability to the entire range of thermomechanical conditions. Thermoelectric heat transfer equation of SMA actuators and the response of one SMA wire under the step and ramp input current in free-stress case have been investigated in the third section. Finally, in the last section the thermoelectric heat transfer and thermomechanical equations of SMA wires coupled with non-linear load deflection behavior of a beam are solved numerically and the beam, as well as wires behavior is shown for some practical cases.

2. NON-LINEAR ANALYSIS OF A FLEXIBLE BEAM UNDER TWO AXIAL FORCES

A real smart structure can be made from several actuators and complex structural members. Because of

the nonlinear and hysteric behavior of shape memory alloy under temperature and stress variation, the prediction of the functionality of such structures in all loading conditions turns out to be complicated. It should be mentioned here that since in shape control applications the wires temperature will often be affected by the resistive heating and the wires electrical current is considered as the control parameters, the control parameter in this paper also is the electrical currents of the wires and the control targets are the wires strain or the wires' connecting point deflections! Knowing the beam behavior under actuation of different actuators can also be helpful to understand the smart structures behavior. In addition, since the tip position of the structure is supposed to be controlled by two SMA actuators, a smart structure composed of an elastic beam and two different SMA wires under their thermal excitation is considered. The arrangement of the beam and the two SMA wires prior and after deformation is schematically shown in Figure 1! Since most of the SMAs undergo a change in behavior under cycling loading [5], it is assumed that the SMA wires have been initially stabilized and then attached to the beam. Incidentally, before attaching the SMA wires to the beam they are subjected to a tensile stress in order to induce some prestrains in wires. Next, one side of the wire.1 and wire.2 is attached to the beam with offset distances d_1 and d_2, respectively. The wire.2 is attached to the tip of the beam while wire.1 is attached to the middle. As stated before, in order to have generality in modeling, the other sides of the wires are fixed to the base at (X_{01},Y_{01}) and (X_{02},Y_{02}) positions, respectively. Increasing the temperature of SMA wires cause martensite to austenite transformation in wires, which creates stress and strain in the beam and as a result deflect it!

Let (ς_1,η_1) and (ς_2,η_2) be the coordinates of points on the beam in which the wires are attached and (x_1,y_1) and (x_2,y_2) are the coordinates of wires end points in the fixed $X-Y$ Cartesian coordinate system, respectively as shown in Figure 2. Also, assume that the pair $(x,w(x))$ defines the coordinate of any points on the beam in the mentioned coordinate system in which the $w(x)$ is the deflection of the point x from the X-axis! Moreover, $w'(x)$ is the slop of the any point of the beam with x coordinate. It is clear from this figure that the relations between x_1,y_1,x_2,y_2 and $\varsigma_1,\eta_1,\varsigma_2,\eta_2$ can be written as:

$$\begin{aligned} x_1 &= \varsigma_1 - d_1 \sin\left(a\tan(w'(\varsigma_1))\right) \\ y_1 &= \eta_1 + d_1 \cos\left(a\tan(w'(\varsigma_1))\right) \\ x_2 &= \varsigma_2 - d_2 \sin\left(a\tan(w'(\varsigma_1))\right) \\ y_1 &= \eta_2 + d_2 \cos\left(a\tan(w'(\varsigma_1))\right) \end{aligned} \quad (1)$$

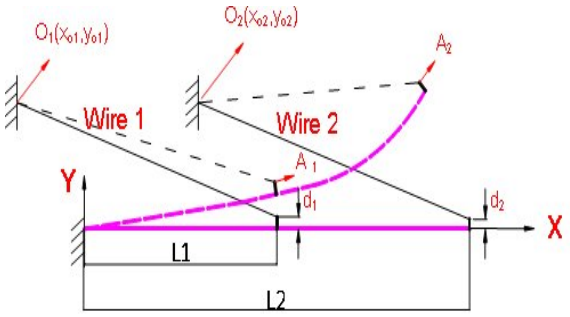

Figure 1. The schematic illustration of the beam structure and SMA wires prior and after deformation.

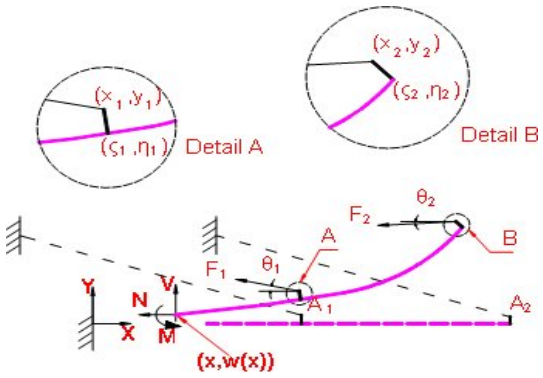

Figure 2. Free body diagram of the deflected beam.

Moreover, the cosines and sinuous of the parameters θ_1 and θ_2, denoted respectively by C_1,S_1,C_2,S_2, are:

$$\begin{aligned} C_1 &= \cos(\theta_1) = \frac{x_1 - x_{01}}{\sqrt{(x_1 - x_{01})^2 + (y_1 - y_{01})}} \\ S_1 &= \sin(\theta_1) = \frac{y_1 - y_{01}}{\sqrt{(x_1 - x_{01})^2 + (y_1 - y_{01})}} \\ C_2 &= \cos(\theta_2) = \frac{x_2 - x_{02}}{\sqrt{(x_2 - x_{02})^2 + (y_2 - y_{02})}} \\ S_2 &= \sin(\theta_2) = \frac{y_2 - y_{02}}{\sqrt{(x_2 - x_{02})^2 + (y_2 - y_{02})}} \end{aligned} \quad (2)$$

By getting moment about point $(x,w(x))$, the distribution of bending moment, M, along the beam span is obtained as:

$$M = \begin{cases} (F_1C_1 + F_2C_2)w(x) - (F_1S_1 + F_2S_2)x + \\ F_1(S_1x_1 - C_1y_1) + F_2(S_2x_2 - C_2y_2) & 0 \le x \le \varsigma_1 \\ F_2C_2w(x) - F_2S_2x + F_2(S_2x_2 - C_2y_2) & \varsigma_1 < x \le \varsigma_2 \end{cases} \quad (3)$$

The differential equation governing the bending moment and the beam deflection is:

$$\frac{-M}{EI} = \kappa = \frac{w''(x)}{(1 + w'(x)^2)^{3/2}} \quad (4)$$

Knowing the two axial forces F_1 and F_2, one cannot find out the deflection $w(x)$ of the beam because there are four unknowns $\varsigma_1,\eta_1,\varsigma_2,\eta_2$ that finding them requires four equations. Thses equations are:

$$w(\varsigma_1)=\eta_1, \quad w(\varsigma_2)=\eta_2$$
$$\int_0^{\varsigma_1}\sqrt{1+(w'(x))^2}dx=L_1, \quad \int_0^{\varsigma_2}\sqrt{1+(w'(x))^2}dx=L_2 \tag{5}$$

The first two of Equation (5) indicate that pair points (ς_1,η_1) and (ς_2,η_2) are on the beam and therefore should satisfy the beam bending equation. The third and fourth equations are the inextensional hypothesis of the beam indicating that the length of the beam remains unchanged in the beam axial direction after bending.

Knowing the two axial forces F_1 and F_2 and by solving the Equations (3-5) iteratively, utilizing the bisection technique, one is able to find out the beam deflections.

3. SIMULATION RESULT OF BEAM EQUATIONS

Before the response of the beam under the thermal actuation of SMA wires is investigated, first the load deflection behavior of the beam is simulated. In order to see the behavior of the beam under different load conditions, a short series of simulation is run with the beam arrangement illustrated in Figure 1. The geometry parameters and material properties of an aluminum beam is given in Table 1 as an example. Since for a beam actuated by one force the nonlinear theory tracks the experimental data more accurately and the linear theory is valid only for small deflections [5], these simulations are run for nonlinear assumptions (i.e. $w'(x)>>0$) that have more generality with respect to linear ones (i.e. $w'(x)\approx 0$).

Figure 3 shows the variation of the end point deflection (point A_2 in Figure 1) with respect to the change in F_1 and F_2. From this figure two points can be born in mind. First, in large F_1 and F_2 forces the system is much nonlinear and sensitive to loading variations; that is, position control at large deflections is greatly difficult. Second, as it turns out the change in the end point deflection with respect to F_2 is more severe than with respect to F_1; i.e., because of the larger moment of F_2 about the base of the beam, the specified variation of F_2, when the same variation in F_1 is enforced, leads to more deflection change in the end point. Thus, it can be inferred that to control the position of the end point it is easier to change F_1 rather than F_2.

This explains why the configuration shown in Figure 1 uses two forces for control position rather than one force. Although the end point position can be controlled by either F_1 or F_2, this brings about two problems. First, if F_2 is applied, albeit the end point can reach to the large deflection, the position control of this point will be difficult. Applying F_1, plus F_2, not only increases the end point workspace (as it is shown in Figure 4), but also its controllability. Second, although the controllability is great, using F_1 cannot lead to the large deflection positions.

TABLE 1. Geometry parameters and material properties of an aluminum beam used for numerical simulations.

Parameter	Symbol	Unit	Value
Length of the beam at connection point with wire.1	L_1	mm	400
Length of the beam at connection point with wire.2	L_2	mm	200
Width	b	mm	25
Thickness	t	mm	1.27
First Force Offset Distance	d_1	mm	5
Second Force Offset Distance	d_2	mm	10
Position of First Force Support	(X_{01},Y_{01})	mm , mm	(0,5)
Position of Second Force Support	(X_{02},Y_{02})	mm , mm	(0,10)
Young modulus	E	GPa	70

4. THERMOMECHANICAL CONSTITUTIVE RELATIONS FOR SMA WIRES

Shape memory behavior in SMAs is caused by a reversible thermoelastic crystalline phase transformation between a high symmetry parent phase (austenite) and a low symmetry product phase (martensite). This phase transformation occurs as a function of both stress and temperature. At zero stress, phase transformation occurs at temperatures denoted by A_s, A_f, M_s and M_f, which respectively represent austenite start, austenite finish, martensite start and martensite finish. At temperatures below M_s, application of stress causes a transformation from 'twinned' martensite to the stress-preferred or 'detwinned' martensite. This process results in large strains at relatively constant stresses. These strains can be completely recovered by heating the material beyond A_f and then cooling without applying any stress. This is called the shape memory effect (SME). On the other hand, at temperatures above A_s, the application of stress causes a transformation from austenite to the detwinned martensite [8]. By removing the stress this process is reversible in a hysteresis loop, and is called pseudoelasticity.

The behavior of SMAs primarily is a function of three variables: stress, strain and temperature, and their corresponding rates. The SMA constitutive models

attempt to describe the SMA behavior as a function of these variables. Most of these constitutive models employ specific material parameters that are determined by experimentation for a particular material.

Several three-dimensional constitutive models have been developed for SMAs. However, none of these models is widely used in engineering applications due to the fact that the developed models are too complicated and need many parameters to be specified. An advantage of 1-D models is that the parameters are engineering-based and simply determined by typical mechanical engineering experiments. In addition, since SMA wires are one-dimensional structures, these three dimensional models should be simplified to acquire application for these 1-D components.

Tanaka model is one of the first constitutive formulations for SMAs [9]. It is assumed that strain, temperature and martensite volume fraction are the only state variables in this model and the stress is calculated as a function of these variables. Furthermore, phase transformation kinetics is expressed in exponential form and is a function of stress and temperature. Liang and Rogers [10] formulated a model based on the rate form of the Tanaka constitutive equation except a cosine model was replaced by the exponential model for the martensite volume fraction.

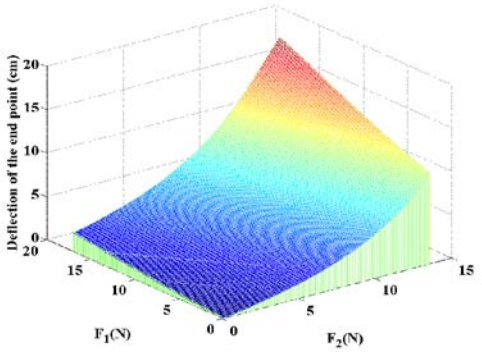

Figure 3. Deflection variation of the end point with F_1 and F_2 changes.

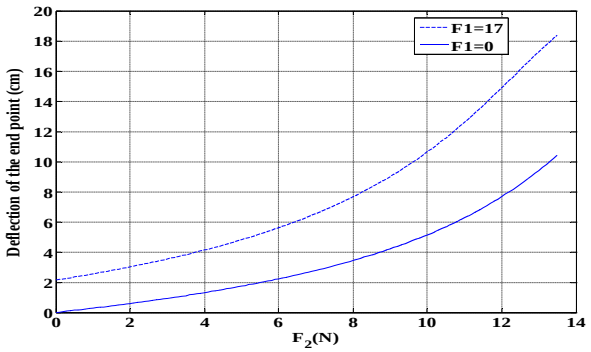

Figure 4. Achieving larger deflection by F_1 interference; the deflection variation of the end point with F_2 changes while F_1 is fixed.

The major drawback for both of the Tanaka and the Liang and Rogers models in their original form is that they only describe the phase transformation from martensite to austenite and its reverse transformation. These models cannot be applied to the detwinning of the martensite that is responsible for the SME at lower temperature, because the SME is caused by the conversion between stress-induced martensite and temperature-induced martensite. This problem was solved by Brinson model [11]. In this model the martensite volume fraction (ξ) is separated into stress-induced (ξ_s) and temperature-induced components (ξ_T):

$$\xi = \xi_s + \xi_T \tag{6}$$

The first form of the constitutive equation in this model, relating the state variable stress (σ), strain (ε) and temperature (T), was:

$$\sigma - \sigma_0 = E(\xi)\varepsilon - E(\xi_0)\varepsilon_0 + \Omega(\xi)\xi_s - \Omega(\xi_0)\xi_{s0} + \Theta(T - T_0) \tag{7}$$

where $(\sigma_0, \varepsilon_0, \xi_0, T_0)$ represent the initial state or original condition of the material and Θ is thermal coefficient of expansion. In this equation E is the module of elasticity and assumed to be a linear function of the martensite volume fraction:

$$E(\xi) = E_A + \xi(E_M - E_A) \tag{8}$$

and Ω is called phase transformation coefficient and is defined:

$$\Omega(\xi) = -\varepsilon_L E(\xi) \tag{9}$$

where ε_L is the maximum recoverable strain. It was shown by Brinson et al. [12] that this constitutive equation could be reduced to the simplified form of:

$$\sigma = E(\xi)(\varepsilon - \varepsilon_L \xi_s) + \Theta(T - T_0) \tag{10}$$

The critical stress-temperature profiles used in Brinson model are shown in Figure 5. The evolution equations for calculation of the martensite fractions according to temperature and stress can now be represented.

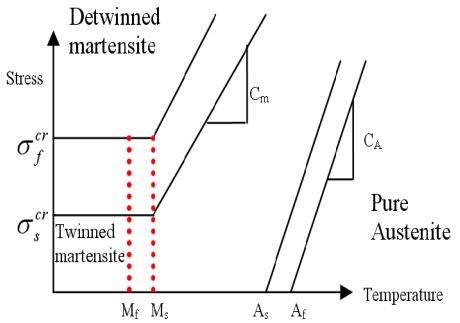

Figure 5. Critical stress–temperature profiles used in Brinson model.

4. 1. Conversion to Detwinned Martensite: For $T > M_s$ & $\sigma_s^{cr} + C_M(T - M_s) < \sigma < \sigma_f^{cr} + C_M(T - M_s)$

$$\xi_s = \frac{1-\xi_{s0}}{2}\cos\left\{\frac{\pi}{\sigma_s^{cr}-\sigma_f^{cr}}[\sigma-\sigma_f^{cr}-C_M(T-M_s)]\right\}+\frac{1+\xi_{s0}}{2}$$
$$\xi_T = \xi_{T0} - \frac{\xi_{T0}}{1-\xi_{s0}}(\xi_s - \xi_{s0}) \quad (11)$$

For $T < M_s$ & $\sigma_s^{cr} < \sigma < \sigma_f^{cr}$

$$\xi_s = \frac{1-\xi_{s0}}{2}\cos\left[\frac{\pi}{\sigma_s^{cr}-\sigma_f^{cr}}(\sigma-\sigma_f^{cr})\right]+\frac{1+\xi_{s0}}{2} \quad (12)$$

$$\xi_T = \xi_{T0} - \frac{\xi_{T0}}{1-\xi_{s0}}(\xi_s - \xi_{s0}) + \Delta_{T\varepsilon}$$

where if $M_f < T < M_s$ and $T < T_0$:

$$\Delta_{T\varepsilon} = \frac{1-\xi_{T0}}{2}\left\{\cos\left[a_M(T-M_f)\right]+1\right\}$$

else

$$\Delta_{T\varepsilon} = 0$$

4. 2. Conversion to Austenite: For $T > A_s$ and $C_A(T - A_f) < \sigma < C_A(T - A_s)$

$$\xi = \frac{\xi_0}{2}\left\{\cos\left[a_A\left(T - A_s - \frac{\sigma}{C_A}\right)\right]+1\right\},$$
$$\xi_s = \xi_{s0} - \frac{\xi_{s0}}{\xi_0}(\xi_0 - \xi), \xi_T = \xi_{T0} - \frac{\xi_{T0}}{\xi_0}(\xi_0 - \xi) \quad (13)$$

In these equations the constants a_A, a_M, b_A, b_M are four material constants in terms of transition temperatures A_s, A_f, M_s, and M_f as:

$$a_A = \frac{\pi}{(A_f - A_s)}, b_A = \frac{-a_A}{C_A}, \quad a_M = \frac{\pi}{(M_s - M_f)}, b_M = \frac{-a_M}{C_M}$$

The original Brinson model [11], in the case when $M_f < T < M_s$ and $\sigma_s^{cr} < \sigma < \sigma_f^{cr}$, can only be used with specific initial conditions, otherwise it gives rise to a physically inadmissible volume fraction ($\xi > 1$). Although after Brinson's original model, Bekker and Brinson developed a kinetics that was robust and did not permit volume fractions to exceed unity [12], Brinson's original model is still widely used in formulae describing the behavior of SMAs. To meet the above conditions, a modification of Brinson's martensite kinetics by Chung et.al. is developed [14]. In this formulation, the Equation (12) is revised as:

For $T < M_s$ and $\sigma_s^{cr} < \sigma < \sigma_f^{cr}$:

$$\xi_s = \frac{1-\xi_{s0}}{2}\cos\left[\frac{\pi}{\sigma_s^{cr}-\sigma_f^{cr}}(\sigma-\sigma_f^{cr})\right]+\frac{1+\xi_{s0}}{2}$$
$$\xi_T = \Delta_{T\varepsilon} - \frac{\Delta_{T\varepsilon}}{1-\xi_{s0}}(\xi_s - \xi_{s0}) \quad (14)$$

where if $M_f < T < M_s$ and $T < T_0$:

$$\Delta_{T\varepsilon} = \frac{1-\xi_{s0}-\xi_{T0}}{2}\cos\left[a_M(T-M_f)\right]+\frac{1-\xi_{s0}+\xi_{T0}}{2}$$

else

$$\Delta_{T\varepsilon} = \xi_{T0}$$

It is shown in literature [15] that this modification satisfies the following statements, regardless of initial conditions:

1) In all condition: $\xi \le 1$.
2) If $\sigma = \sigma_f^{cr}$ then $\xi_s = 1$.
3) If $T = M_f$ then $\xi = 1$.

In this paper, for analysis of the SME and superelastic behavior of SMA components, the Brinson model with the corrected evolution kinetics developed by Chung et.al is applied. In order to obtain the required thermomechanical properties of a Ni–Ti alloy, experimental measurements were carried out on a FlexinolTM actuator wire, manufactured by Dynalloy, Inc. For the experiment, one-way shape memory, 0.01 inch diameter (0.254 mm), low temperature (70 ◦C), Ni–Ti SMA actuator wire has been selected. The details of these tests are reported in a separate paper [15] and the experimentally derived parameters related to Brinson model are tabulated in Table 2.

5. THERMOELECTRIC HEAT TRANSFER EQUATION OF SMA ACTUATORS

In most shape and position control applications that SMA wires are used as actuators their temperature is changed more by resistive heating of electrical currents rather than the surrounding medium; i.e., in the former, the electrical current is the control input while in the latter the SMA wire temperature. Therefore, the heat transfer problem of a thin SMA wire actuator with resistive heating is investigated in the current study.

Shu et al. [3] showed that for the long wires, used in many control applications, the equation governing the aforementioned problem can be reduced into the following simplified equation:

$$C_v(T,\sigma)\frac{\partial T(t)}{\partial t} = -\frac{4}{D}h(T)[T(t) - T_{amb}] + \rho_e J^2 \quad (15)$$

where $T(t)$ is the temperature of the wire at time t, D the diameter of the wire, ρ_e the electrical resistivity of the wire, J the magnitude of the current density (i.e. I/A where A is the wire cross section area), T_{amb} the ambient temperature, $C_v(T,\sigma)$ the heat capacity and $h(T,D)$ the *convective heat coefficient*.

If in this equation the heat capacity is assumed to be fixed, the term $q(\partial\xi/\partial t)$ (where q is a constant index

representing the total latent heat in the course of transformation and ξ the martensite volume fraction) should be added to this equation. However, by considering the inconstant heat capacity, this term is not needed any more.

Bhattacharyya et al. [16] proposed an empirical relation describing the dependence of C_v on T and σ as follows:

$$C_v = \begin{cases} if \left\{ M_f + \frac{\sigma}{C_M} \le T \le M_s + \frac{\sigma}{C_M} \right\} \Rightarrow \\ C_v^0 + q \frac{\ln(100)}{(M_s - M_f)} \exp \\ \left[-\frac{2\ln(100)}{(M_s - M_f)} \left| T - 0.5(M_s + M_f + \frac{2\sigma}{C_M}) \right| \right] \\ else \Rightarrow \qquad C_v^0 \end{cases} \quad (16)$$

for the forward transformation, and

$$C_v = \begin{cases} if \left\{ A_s + \frac{\sigma}{C_A} \le T \le A_f + \frac{\sigma}{C_A} \right\} \Rightarrow \\ C_v^0 + q \frac{\ln(100)}{(A_f - A_s)} \exp \\ \left[-\frac{2\ln(100)}{(A_f - A_s)} \left| T - 0.5(A_s + A_f + \frac{2\sigma}{C_A}) \right| \right] \\ else \Rightarrow \qquad C_v^0 \end{cases} \quad (17)$$

for the reverse transformation. It should be mentioned here that these equations are somewhat different from the equations that used in their paper because, as discussed in the previous sections, stress has a profound effect on the transformation temperature but in their study, Bhattacharyya et al. overlooked this effect on transformation temperature.

The convection coefficient as a function of the wire temperature and its diameter is as follows [3]:

$$h(T, D) = \frac{k}{D} Nu \quad (18)$$

TABLE 2. Experimentally derived SMA parameters and properties.

Material Parameter	Value	
M_f	43.9	[°C]
M_s	48.4	[°C]
A_s	68	[°C]
A_f	73.75	[°C]
C_A	6.73	[MPa/°C]
C_M	6.32	[MPa/°C]
ε_L	4.1	[%]
E_A	31.5	[GPa]
E_M	20	[GPa]
σ_s	25	[MPa]
σ_f	78	[MPa]

where k is the thermal conductivity of the surrounding air and Nu the average Nusselt number for free convection of the SMA wire. In this empirical model, the dimensionless Nusselt number can be related to the Rayleigh number ($Ra = Gr\,Pr$) as follows:

$$Nu = C\,Ra^m \quad (19)$$

where the dimensionless Grashof number Gr and the Prandtle number Pr are given as [3]:

$$Gr = \frac{2(T - T_\infty) g D^3}{(T + T_\infty) \upsilon^2}, \qquad \Pr = \frac{\mu C_p}{k} \quad (20)$$

In Equation (20), g is the gravitational acceleration ($g = 9.81 m\,s^{-2}$), υ, μ, C_p and k the kinematic viscosity, viscosity, heat capacity at constant pressure and thermal conductivity of the surrounding air, respectively.

For obtaining *C* and *m* in Equation (19), the value of h should be correlated with a set of experimental data. using a generalized reduced gradient algorithm (GRG) to minimize the average fit error with respect to the collected data, Pathak et al. [18] found the following value for these values for the two Rayleigh regimes:

$$\begin{aligned} &C = 0.875,\ m = 0.038 \qquad for\ 10^{-10} < Ra < 10^{-2} \\ &C = 1.477,\ m = 0.142 \qquad for\ 10^{-2} < Ra < 10^{2} \end{aligned} \quad (21)$$

Since it is found that the Ra number for the wire in hand is in the second Rayleigh regime, the corresponding *C* and *m* values are chosen.

It should be mentioned that the physical parameters of Equations (18) and (20) should be evaluated at the average temperature ($T_{ave} = \frac{T + T_{amb}}{2}$). The properties of air at atmospheric pressure are obtained form Table A-5 of [17]. These properties are tabulated in Table 3.

Since the working temperature of the SMA wire in hand is between $40^\circ C$ (below $M_f = 44^\circ C$) and $140^\circ C$ (the austenite finish temperature at $\sigma = 450 MPa$) and by assuming the temperature of surrounding air as $T_{amb} = 20^\circ C$, the average temperature is between $30^\circ C \le T_{ave} \le 80^\circ C$ and the data of this table is sufficient. By assuming that the value of these parameters is changed linearly between 300°C and 400 °C, the value of Grashof number Gr and the Prandtle number Pr in any temperature can be easily computed by Equation (20). Then by using Equations (18-21), the convection coefficient can be obtained in each temperature in the mentioned working temperature range.

Figure 6 shows the change of convective coefficient with the temperature of SMA wire. As it is seen the convective heat transfer increases as the wire temperature is increased. It is due to the fact that by rising the wire temperature (by assuming the fixed ambient temperature) the rate of heat transfer climbs

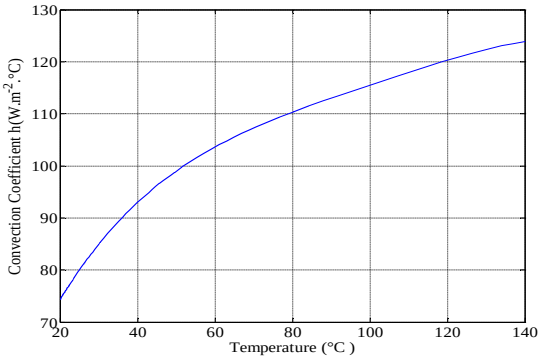

Figure 6. Convective heat transfer coefficient of SMA wire versus temperature.

due to increase of temperature difference between the actuator and the ambient. It is found that the change of h with temperature can be fitted by a 4-degree polynomial and the maximum error of this fitting is below 0.15°C. This fitted equation is:

$$h(T) = -4.034\times10^{-7}\,T^4 + 0.0001654\,T^3 - 0.02586\,T^2 + 2.071\,T + 41.96 \qquad T(^\circ C)\ and\ h(W.m^{-2}.^\circ C^{-1}) \tag{22}$$

In order to solve the Equation (15), three other parameters (C_{v0}, q and ρ_e) should be obtained. By performing the differential scanning calorimetric (DSC) test, the first and second parameters are obtained as:

$$C_{v0} = 2.046\times10^{6}\,(J.m^{-3}.^\circ C^{-1})$$

$$q = 0.0656\times10^{9}\,J.m^{-3}$$

Although the electrical resistivity is also a function of the wire temperature , its change with temperature is not considerable (below 8%) and lack of reliable data also forces us to select the average resistivity of austenite and martensite phases reported by manufacture (Dynalloy, Inc) and this was: $\rho_e = 80\times10^{-8}\,\Omega.m$. The related heat transfer parameters are summarized in Table 4.

Since the heat capacity is a function of temperature and stress (Equations (16) and (17)), by knowing the current of the wire solely, in order to obtain the temperature profile, it is not possible to solve Equation (15) independently from constitutive equation of SMAs and nonlinear beam equation, Therefore, this equation should be coupled with other equations and then all of coupled equations should be solved simultaneously.

In special cases, if the heat capacity and convection coefficient are assumed to be fixed then the Equation (15) will be simplified into the following equation:

$$C_v\frac{\partial T(t)}{\partial t} = -\frac{4}{D}h\left[T(t) - T_{amb}\right] + \rho_e J^2 \tag{22}$$

By getting Laplace transformation, the linear transfer functions between J^2 and T may be written as:

$$G(s) = \frac{\overset{\Delta}{T}(s)}{J^2} = \frac{\frac{\rho_e D}{4h}}{1+\frac{C_v D}{4h}s} \tag{23}$$

The time constant and the settling time of the response in this transfer function, as well as the steady-state value attained for a step current input, respectively, are:

$$\tau = \frac{C_v D}{4h}, \qquad t_{settling\ time} \approx \frac{C_v D}{h}, \qquad T_{ss} = \lim_{s\to 0} sG(s).\frac{1}{s} = \frac{\rho_e D}{4h}J^2 \tag{24}$$

These equations can be helpful to obtain the approximate input current to reach maximum desired temperature, and the approximate time that the current should persist (for step current input) before running the simulation. For example, in special cases, by assuming

$C_v = C_{v0} = 2.046\times10^{6}\,(J.m^{-3}.^\circ C)$,

$h = h(T = 55^\circ C) = 101.4656\ (W.m^{-2}.^\circ C^{-1})$,

$D = 2.54\times10^{-4}\,m$, and by supposing that the maximum desired temperature is $T_{ss} = 140^\circ C$, the following values are obtained for the time constant, settling time and the step input current:

$$\tau \approx 1.29(\text{sec}), \quad t_{settling\ time} \approx 5.13(\text{sec}), \quad I_{step} \approx 0.85(A)$$

In free stress case (i.e. $\sigma = 0 Mpa$) and under the step and ramp input current, the corresponding temperature profile is obtained (by numerical solving of Equation (15)) and is shown in Figure 7.

As it is seen from this figure, the total cooling time is more than the corresponding heating time (for step input: $t_{heating} \approx 5\,\text{sec}, t_{cooling} \approx 10$ sec and for ramp input $t_{heating} \approx 9\,\text{sec}, t_{cooling} \approx 14\,\text{sec}$).

TABLE 3. Properties of air at atmospheric pressure at 300, 350 and 400 K [17].

$T(K)$	$C_p(\frac{KJ}{Kg.^\circ C})$	$\mu(10^{-5}\frac{Kg}{m.s})$	$\upsilon(10^{-6}\frac{m^2}{s})$	$k(\frac{W}{m.^\circ C})$
300	1.0057	1.8462	15.69	0.02624
350	1.0090	2.075	20.76	0.03003
400	1.0140	2.286	25.90	0.03365

TABLE 4. Heat transfer parameters used for simulations.

Material Parameters	Value	Unit
C_{v0}	2.046×10^{6}	$J.m^{-3}.^\circ C^{-1}$
q	0.0656×10^{9}	$J.m^{-3}$
ρ_e	80×10^{-8}	$\Omega.m$
T_{amb}	20	$^\circ C$
$h(T)$	Refer to Equation (22)	$W.m^{-2}.^\circ C^{-1}$

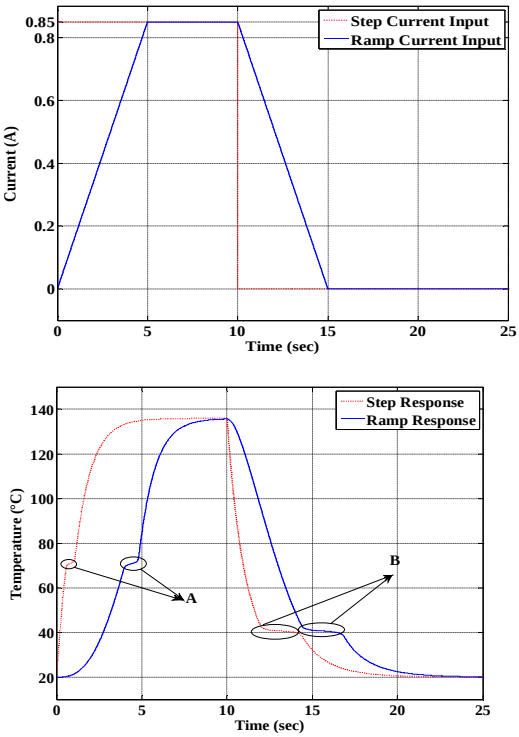

Figure 7. Response of the SMA actuator under electrical different current profile in free stress case.

It is due to this fact that the heating is mostly controlled by the magnitude of the input current term $\rho_e J^2$, while the cooling rate depends only on the heat convection between the SMA wire and surrounding air and it is a linear function of the temperature difference between the actuator and the ambient temperature (the $(-\frac{4}{D}h(T)[T(t)-T_{amb}])$ term). The areas specified by A and B are the regions where the specific heat changes in the reverse and forward transformations. It seems, in this special simulation, that the corresponding time to these regions is shorter than the total heating or cooling time and assuming constant specific heat does not lead into much error.

However, as will be shown in the later simulations, in the presence of stress, this time is not ignorable and assuming constant specific heat yields erroneous results.

6. SIMULATION OF STRUCTURAL RESPONSE AND RESULTS

Computer simulations of the SMA actuated beam model were performed in MATLAB. Block diagram of the model is shown in Figure 8. As it is seen from this figure, the inputs of the SMAs actuated beam model are the wires currents while its output is the strain of the corresponding wires. The geometry of the aluminum beam to be investigated in this study is given in Table 1. In addition, the material parameters of the SMA actuator wires are given in Table 2.

Since different initial conditions of each SMA wire (different detwinned martensite volume fraction and prestress) as well as different algorithms of heating and cooling of each SMA, affect the behavior of stress-strain in each wire and the beam behavior, several cases are studied for simulation. In the initial state of each parameter, the superscript '1' refers to the wire-1 and the superscript '2' refers to the wire-2. To observe the effect of considering or neglecting the SMA wire-1 on the variation of parameters, two graphs are illustrated in some figures: one by considering the effect of SMA wire-1 (entitled by Case-A) and another by neglecting the effect of SMA wire-1 (entitled by Case-B); i.e. assuming that only wire-2 is connected to the beam.

In addition, in all simulations the ON-OFF current is applied to the wires. The duration of ON-section of the current at each simulation is selected in such a way that both wires temperature saturate to their steady state. Therefore, it is not same for all simulations and there is a slight difference between these duration times. Also, the OFF-section duration of the current is selected in such a way that both wires temperature reach to the ambient temperature.

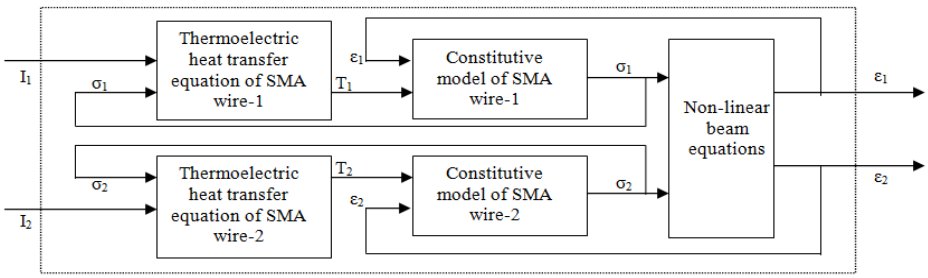

Figure 8. Block diagram of the flexible beam actuated by SMA actuators.

6. 1. First Simulation

Initial condition:

$$\left\{\begin{matrix}\xi_{s0}^{1}=1,\xi_{T}^{1}{}_{0}=0,\sigma_{0}^{1}=100Mpa\\ \xi_{s0}^{2}=0.5,\xi_{T}^{2}{}_{0}=0.5,\sigma_{0}^{2}=0Mpa\end{matrix}\right\}$$

Heating Algorithm :

$$\left\{\begin{matrix}\mathrm{T}^{1}=20^{\circ}C\,(\mathrm{fixed})\\ \mathrm{T}_{0}^{2}=20^{\circ}C\,,\mathrm{I}^{2}=0.85A\,(ON\;-OFF\;current)\\ (t_{heating}=13.53\mathrm{sec}\;\&\,t_{cooling}=17.64\mathrm{sec})\end{matrix}\right\}$$

In order to investigate the sole effect of thermal actuation of wire-2 on the beam behavior, in this simulation the temperature of wire-2 is changed by applying the input step current 0.85A while no current applied to wire-1. As a result, the temperature of wire-1 is fixed at 40°C (with 100 MPa initial prestress) and the temperature of wire-2 is increased from 40°C to 136°C.

In Figure 9, the stress of wire-2 is plotted as a function of its temperature changes for Case-A and Case-B. The light dashed lines on the plot indicate the transformation strips displayed earlier in Figure 5. It is seen from this figure that even in this simulation the wire-1 is inactive but ignoring it can contribute to erroneous prediction of stress in the wire-2. In other words, in the cases where the effect of wire-1 is neglected, the model over predicts the stress of wire-2. As will be shown later this matter is more severe in the cases that the SMA wire-1 has thermal actuation beside the SMA wire-2. Similarly, in Figure 10, the stress of wire-1 is shown as a function of the wire-2 temperature when the effect of SMA wire-1 is not neglected (Case-A). In the same way, Figure 11 shows the deflection of the end point as a function of the wire-2 temperature changes, in the heating and cooling process, for Case-A and Case-B. It is seen in this figure that ignoring the effect of wire-1 underpredicts the deflection of the end point.

Correspondingly, Figure 12 shows the change of stress-induced (ξ_s) martensite fraction of wire-2 as a function of the wire-2 temperature for Case-A and Case-B. As it is seen from this figure there is not any significant difference between the result of Case-A and Case-B for this special simulation. Likewise, in Figure 13 the temperature change of wire-2 as a function of time is shown for Case-A and Case-B.

By comparing the results of Case-A and Case-B in this simulation it is concluded that for applications where precise modeling is required the effect of all SMA wires should be considered, even if some of them are inactive and have no thermal actuation. Since Case-A consider the effect of inactive SMA wire-1 and has more precise result, the subject of the following paragraphs is Case-A.

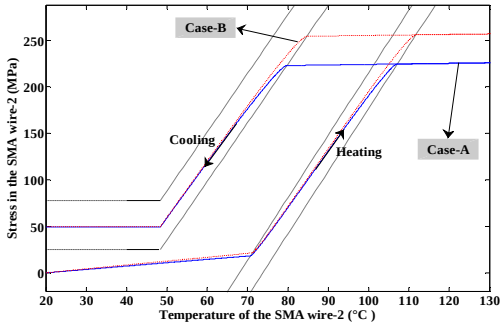

Figure 9. Stress in the SMA wire-2 as a function of its temperature for Case-A and Case-B in the first simulation.

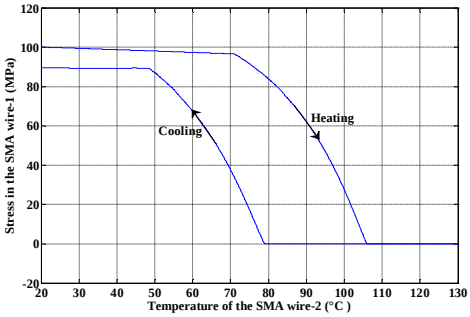

Figure 10. Stress in the SMA wire-1 as a function of the SMA wire-2 temperature for the first simulation.

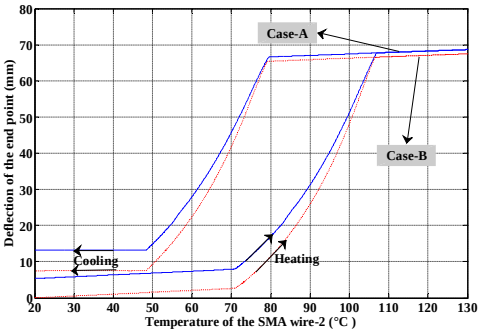

Figure 11. Deflection of the end point as a function of the SMA wire-2 temperature for Case-A and Case-B in the first simulation.

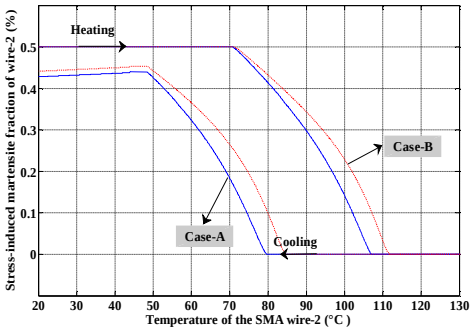

Figure 12. Stress-induced (ξ_S) martensite fraction of the SMA wire-2 as a function of its temperature for Case-A and Case-B in the first simulation.

This is just simulated to show the sole effect of thermal actuation of one wire on the beam behavior. To investigate the behavior of the beam under the both wire thermal actuations there are infinite patterns.

The same thermal actuation for both of the wires turns out to be the simplest way in the first glance but it has ample practical applications, especially in the control processes. Further explanation of this is beyond the scope of this paper.

In addition, there are infinite selections for initial stress-induced marteniste fraction (ξ_s) of wires. However, since reaching to the larger deflection of beam is the goal of this paper we focus on the fully detwinned ($\xi_s = 1$) martensite for initial state of the both SMA wires. When the simulation results for this case (initial condition: $\xi_{s0}^{1}, \xi_{s0}^{2} = 1, \sigma_0^1, \sigma_0^2 = 0$ and heating algorithm: $I^1 = I^2 = 0.85A\,(ON - OFF\ current)$) is investigated, it is seen (Figure 14) that the full phase transformation in the heating process only occurs for the second wire and the first wire does not exit from the phase transformation state (between martensite and austenite phase) even with increasing the wires temperatures up to $150^{\circ}C$. This is due to the fact that the stress-temperature profile for this wire is nearly parallel to phase transformation strips and increasing the wire temperature only increases the stress in wire-1 without departing it from this phase transformation state. Therefore, it is concluded that this simulation is not an appropriate case in this study.

To solve this problem, after several simulations it is concluded that for the same thermal actuation of the both wires, two solutions can be proposed. First, decreasing the initial stress-induced marteniste fraction of the wire-1 and second, enlarging the length of the wire-2 from the behind of the base in such a way that the connection point of wire-2 with the base (point Q_2 in Figure 1) does not change and the comparison with the previous obtained data remains valid.

The following second simulation is selected for the first solution and third simulation is selected for the second solution.

6. 2. Second Simulation

Initial Condition : $\left\{\begin{matrix} \xi_{s0}^{1} = 0.6, \xi_{T0}^{1} = 0.4, \sigma_0^1 = 0 \\ \xi_{s0}^{2} = 1, \xi_{T0}^{2} = 0, \sigma_0^2 = 0 \end{matrix}\right\}$,

Heating Algorithm :

$$I^1 = I^2 = 0.85A\,(ON - OFF\ \ current)$$

$$(t_{heating} = 21.18\ \text{sec}\ \ \&\ t_{cooling} = 38.82\ \text{sec})$$

As discussed before the initial stress-induced marteniste fraction of the wire-1 is decreased to 0.6 in this case in order to have full phase transformation for both wires in the heating and cooling processes. Figure 15 shows the stress of SMA wire-2 as a function of its temperature for Case-A and Case-B. Also, in Figure 16 the stress of SMA wire-1 is plotted as a function of its temperature when the effect of this wire is not neglected (Case-A). Similarly, in Figure 17 the variation of wires temperature is plotted as a function of time in Case-A and Case-B. Correspondingly, Figure 18 shows the deflection of the end point as a function of time in the entire heating and cooling process for both aforementioned cases.

Since both of the SMA wires are active and both of them have thermal actuation, the difference between the result of Case-A and Case-B is significant.

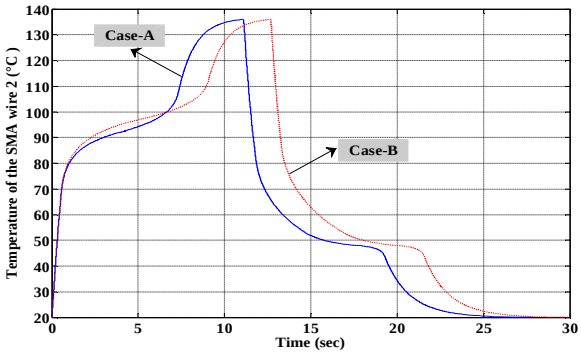

Figure 13. Temperature change of the wire-2 as a function of time for Case-A and Case-B in the first simulation.

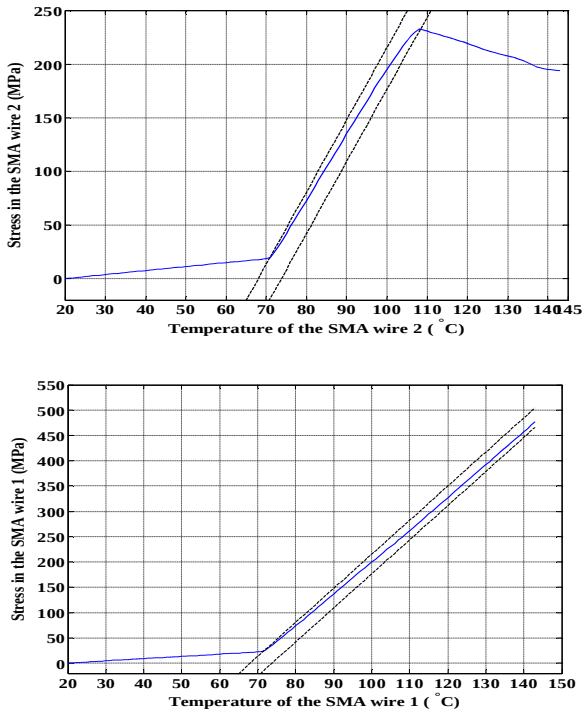

Figure 14. Stress in each SMA wire as a function of their corresponding temperature changes.

In other words, when the effect of SMA wire-1 is neglected in the simulation (Case-B) the model over-predicts the stress of SMA wire-2 while under-predicts the deflection of the end point. It is comprehensible because when the sole actuation of one wire is considered in analysis, the whole of actuation task should be done by one wire and its predicted stresses raises with respect to a case where two wires have thermal actuation. In addition, it cannot yield to larger deflection of beam, and the deflection of the beam is under-predicted. It clearly shows the advantage of using two active SMA wires for deflecting a beam: reaching larger deflection with less stress of each SMA wire.

It is also important to express this point that despite the stress-induced (ξ_s) marteniste fraction of wire-1 is only 0.6 and not 1, the maximum end point deflection for this simulation (Case-A) is 127.4 mm and it is about 18 mm more than the first simulation where there was only one wire actuation. It is also seen, as observed before in the first simulation, the cooling process duration is longer than the heating process duration.

6. 3. Third Simulation

Initial Condition : $\xi_{s0}^{\ i}=1, \xi_{T0}^{\ i}=0, \sigma_0^i=0; i=1,2.$

Heating Algorithm :

$I^1 = I^2 = 0.85A$ $(ON-OFF\ current)$

$(t_{heating}=21.88\sec\ \&\ t_{cooling}=46.37\sec).$

$\text{Added Length to Wire 2} = 0.55\,\text{m}.$

As discussed before, in this simulation the length of wire-2 is enlarged in such a way that the connection point of wire-2 with the base (point Q_2 in Figure 1) does not change. This added length for wire-2 is selected in such a way that if the stress-induced (ξ_s) marteniste fraction of the both wires is selected the maximum (i.e. $\xi_s=1$, in order to reach the maximum deflection for the end point) the full phase transformation occurs for both wires. Figure 19 shows the stress of SMA wire-2 as a function of its temperature for Case-A and Case-B.

Similarly, in Figure 20 the stress of SMA wire-1 is plotted as a function of its temperature when the effect of this wire is not neglected (Case-A). Correspondingly, in Figure 21 the variation of wire temperature is plotted as a function of time in Case-A and Case-B. In the same way, Figure 22 shows the deflection of the end point as a function of the SMA wires temperature in Case-A and Case-B.

Similar to the second simulation, the difference between the results of Case-A and Case-B is severe and neglecting the effect of the wire-1 over predicts the stress of SMA wire-2 while under-predicts the deflection of the end point.

It is also important to express this point that since the stress-induced (ξ_s) marteniste fraction of both SMA wires is 1, the maximum end point deflection for this simulation (Case-A) is 190 mm and it is about 80.6 mm more than the first simulation (74% increase) where there was only one wire actuation. This clearly shows the effect of one excess wire actuation in reaching large deflection for flexible structures. It is also seen from Figure 20, as observed in the first and second simulations; the cooling process duration is longer than the heating process duration.

It should be noted here that all of figures shown so far were only the first cycle response of the beam under the wires thermal actuation. Figure 23 shows the stress of SMA wires as a function of their corresponding temperatures by the subsequent second cycle actuation of SMA wires in third simulations (Case-A). Also, in Figure 24 the deflection of the end point is plotted as a function of time. The initial values of stresses, strains, deflections, etc. in this simulation are selected by the corresponding value obtained at the end of the first cycle simulation. As it is seen from these figures, at the end of the second cycle all of the variables come back to their corresponding initial values. This fact is valid for all subsequent cycles after the first cycle.

7. CONCLUSION

In this paper, some drawbacks of the researches conducted on modeling of smart structures actuated by externally-attached SMA actuators have been resolved and the nonlinear modeling of a flexible beam actuated by two active SMA actuators was carried out. Nonlinear formulation of a flexible beam under two applied forces was first derived. Although, in the view of control, the tip deflection control of a beam can be achieved by only one wire but the sensitivity of the system to the actuation force of that SMA is great and this yields to difficult controllability of the system. Therefore, increasing the actuator number plays an important role in improving the degree of controllability of a beam. Using more than one actuator has also the advantage that shape control is accessible instead of solely position control of one point.

Next, the Brinson thermomechanical constitutive equation of SMA wires was reviewed due to its simplicity and its applicability to the entire range of thermomechanical conditions. In addition, the thermoelectric heat transfer equation of SMA actuators was presented. Finally, the Brinson constitutive model and heat transfer equations of SMA materials were coupled with the nonlinear beam behavior, and the coupled system of equations was numerically solved for some particular practical cases.

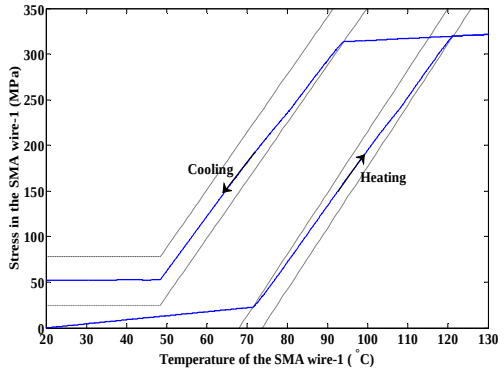

Figure 15. Stress in the SMA wire-1 as a function of its temperature for the second simulation.

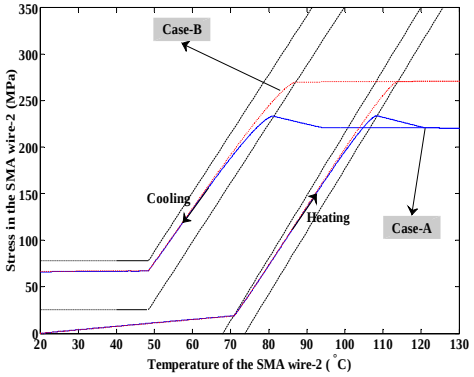

Figure 16. Stress in the SMA wire-2 as a function of its temperature for Case-A and Case-B of the second simulation.

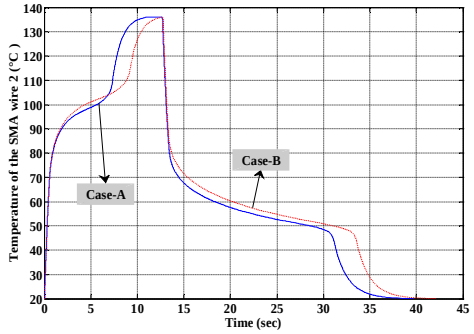

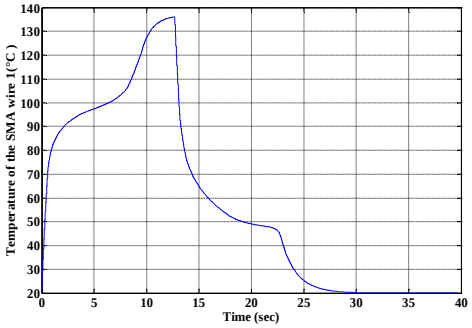

Figure 17. Temperature changes of each SMA wire as a function of time for the second simulation.

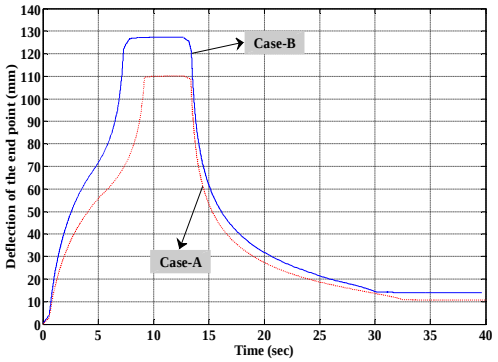

Figure 18. Deflection of the end point as a function of time for Case-A and Case-B in the second simulation.

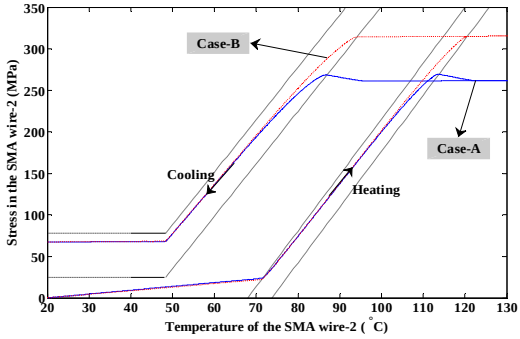

Figure 19. Stress in the SMA wire-2 as a function of its temperature for Case-A and Case-B in the third simulation.

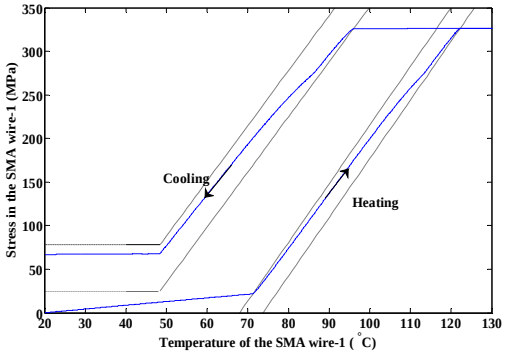

Figure 20. Stress in the SMA wire-1 as a function of its temperature in the third simulation.

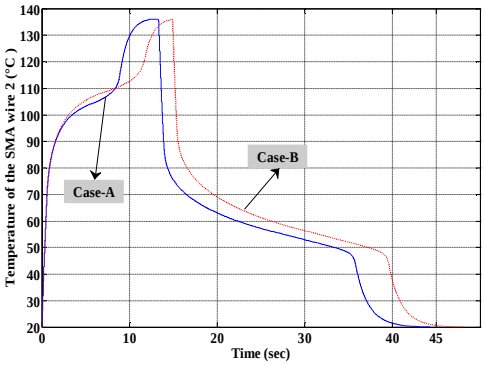

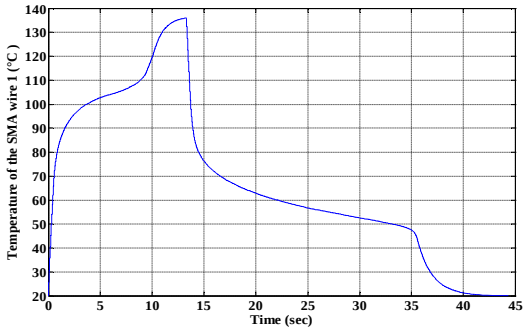

Figure 21. Temperature changes of each SMA wire as a function of time for the third simulation.

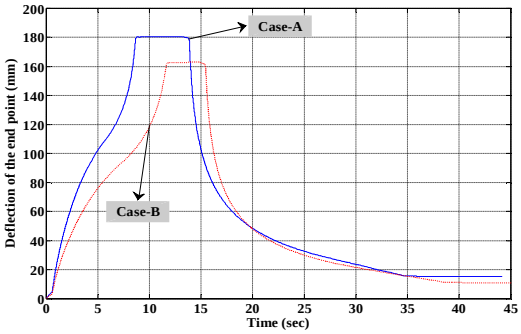

Figure 22. Deflection of the end point as a function of time for Case-A and Case-B in the third simulation.

``

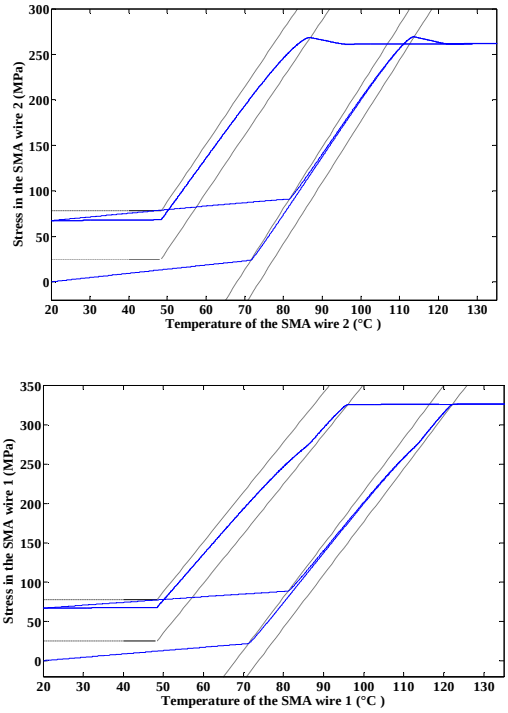

Figure 23. Stress in each SMA wires as a function of the wires temperature in the second cycle of actuation for the third simulation.

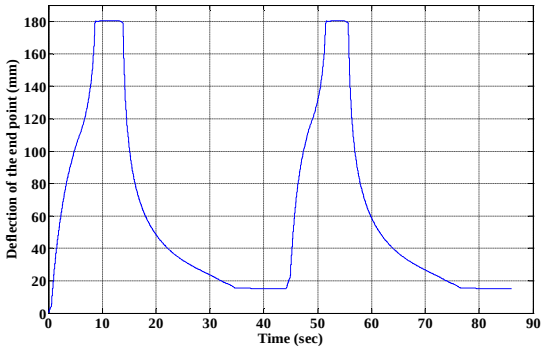

Figure 24. Deflection of the end point as a function of time in the second cycle of actuation for the third simulation.

It was shown that after this first thermal cycle, the magnitude of the all parameters did not reach to their original initial value. It means that the cold states of the wires did not yield to the same beam shape as their hot states and so the beam did not recover its original shape. This occurred only in the first cycle of heating and cooling of wires and as it was shown that in the subsequent cycles the hot and cold shapes of the beam are the same. It was also seen that in the case where two SMA actuators are used, the maximum end point deflection increase 74% with respect to the case where only one actuator is used. This property shows the advantage of the beam model mentioned in reaching large deflection states.

It is also seen that in the cases where there are two active SMA wires and both of them have thermal actuation, the results are significantly differ from the result where the main SMA wire is solely considered and the effect of the other is ignored. This different result is observed even in the cases where one of the wires is active and the other is inactive. It means that in order to have precise result the effect of all active and inactive SMA wires should be considered (like diagnostic configurations). It is also shown that if the effect of some of the SMA wires is neglected the stress in other wires is overpredicted and the deflection of beam is underpredicted with respect to the precise model.

The methodology employed in this paper can be easily extended to the complicated smart structure with externally-attached SMA wires. In addition, the appropriate parameters of these smart structures such as the geometry of structure, the arrangement and the material properties of SMA actuator wires can be selected by this method. Furthermore, the behavior of this smart structure can be easily simulated before the manufacture process and the optimal value of those mentioned parameters could be selected easily.

8. REFERENCES

1. Lagoudas, D. C., 2008, Shape Memory Alloys: Modeling and Engineering Application, Springer, College Station, USA, Chap. 1.
2. Chaudhry, Z., and Rogers, C. A., "Bending and Shape Control of Beams Using SMA Actuators," *Journal of Intelligent Material Systems and Structures*, Vol. 2, (1991), 581–602.
3. Shu, S. G., Lagoudas, D. C., Hughes, D., and Wenx, J. T., "Modeling of a Flexible Beam Actuated by Shape Memory Alloy Wires," *Smart Materials and Structures*, Vol. 6, (1997), 265–277.
4. Boyd, J. G., and Lagoudas, D. C., "Thermomechanical Response of Shape Memory Composites," *Journal of Intelligent Material Systems and Structures*, 5, (1994), 333–46.
5. Brinson, L. C., Huang, M. S., Boller, C., and Brand, W., "Analysis of Controlled Beam Deflection Using SMA Wires," *Journal of Intelligent Material Systems and Structures*, Vol. 8, (1997), 12–25.
6. Moallem, M., "Deflection Control of a Flexible Beam Using Shape Memory Alloy Actuators," *Smart Materials and Structures*, 12, (2003), 1023–1027.
7. Sohn, J. W., Han, Y. M., Choi, S. B., Lee, Y. S., and Han, M. S., "Vibration and Position Tracking Control of a Flexible Beam Using SMA Wire Actuators," *Journal of Vibration and Control*, Vol. 15, No. 2, (2009),263–281.
8. Prahlad, H., and Chopra, I., "Comparative Evaluation of Shape Memory Alloy Constitutive Models with Experimental Data," *Journal of Intelligent Material Systems and Structures*, Vol. 12, (2001), 383-395.
9. Tanaka, K., "A Thermomechanical Sketch of Shape Memory Effect: One- Dimensional Tensile Behavior," *Res. Mechanica*, Vol. 18, (1986), 251–263.
10. Liang, C., and Rogers, C. A., "One-Dimensional Thermomechanical Constitutive Relations for Shape Memory Material," *Journal of Intelligent Material Systems and Structures*, Vol. 1, (1990), 207–234.
11. Brinson, L. C., "One-Dimensional Constitutive Behavior of Shape Memory Alloys: Thermomechanical Derivation with Non-Constant Material Functions," *Journal of Intelligent Material Systems and Structures*, Vol. 4, (1993), 229–242.
12. Brinson, L. C., and Huang, M. S., "Simplifications and Comparisons of Shape Memory Alloy Constitutive Models," *Journal of Intelligent Material Systems and Structures*, Vol. 7, (1996), 108–114.
13. Bekker, A., and Brinson, L. C., "Phase Diagram Based Description of the Hysteresis Behavior of Shape Memory Alloys,'' *Acta Materialia*., Vol. 46, No.10, (1998) ,3649–3655.
14. Chung, J., Heo, J., and Lee, J., "Implementation Strategy for the Dual Transformation Region in the Brinson SMA Constitutive Model," *Journal of Intelligent Material Systems and Structures*, Vol. 16, (2007), N1-N5.
15. Zakerzadeh, M. R., and Salehi, H., "Comparative Analysis of Some one-Dimensional SMA Constitutive Models for a Ni-Ti Wire for Shape Control Applications with Experimental Data," *Proceeding of 20th Int. Conf. on Adaptive Structures and Technologies, Hong Kong*. (2009).
16. Bhattacharyya, A. Lagoudas, D. C., Wang, Y., and Kinra, V. K., "On The Role Of Thermoelectric Heat Transfer In The Design Of SMA Actuators: Theoretical Modeling And Experiment," *Smart Materials and Structures*, Vol. 4, (1995), 252-263.
17. Holman, J. P., 2001, Heat Transfer, McGraw-Hill, 9th ed.
18. Pathak, A., Brei, D., and Luntz, J., 2010, "Transformation Strain Based Method for Convective Heat Transfer Characterization from Shape Memory Alloy Wires," *Smart Materials and Structures*, Vol. 19, No. 3, 035005-035015.

Nonlinear Analysis of a Flexible Beam Actuated by a Couple of Active SMA Wire Actuators

H. Sayyaadi, M. R. Zakerzadeh

School of Mechanical Engineering, Sharif University of Technology, Tehran , P.O. Box 11155-9567, Iran

ARTICLE INFO

Article history:
Received 06 June2010
Received in revised form 03 September 2012
Accepted 19 April 2012

Keywords:
Nonlinear Modeling
Flexible Beam
SMA Actuators

چکیده

دو روش برای استفاده از سیم‌های آلیاژ حافظه‌دار به‌عنوان عملگر جهت کنترل شکل سازه‌های انعطاف‌پذیر وجود دارد: یکی استفاده از این سیم‌ها درون لایه کامپوزیتی و دیگری نصب خارجی آن‌ها. به دلیل این‌که در حالت نصب به‌صورت خارجی عملگر در فواصل بیشتری نسبت به تار خنثی می‌تواند قرار گیرد، ممان خمشی بیشتری ایجاد کرده و در نتیجه سازه تغییر شکل بیشتری می‌تواند پیدا کند. دراین پیکربندی همچنین به‌دلیل نرخ جابه‌جایی بالاتر، سیم حافظه‌دار سریع تر خنک شده و در نتیجه می‌توان با فرکانس بالاتری سازه را تحریک کرد.

اگرچه مدلسازی سازه‌های ترکیبی با سیم‌های حافظه‌دار بسیار مورد بررسی قرار گرفته‌اند، ولی تمامی این مطالعات دارای ضعف‌هایی می‌باشند که نادیده گرفتن آن‌ها می‌تواند باعث ایجاد خطای بسیار بین نتایج تئوری و تجربی شود. در تحقیق حاضر محدودیت‌های مطالعات قبلی برطرف شده و مدلسازی یک تیر انعطاف‌پذیر تحریکی توسط دو سیم حافظه‌دار فعال مورد بررسی قرار گرفته است. معادلات ترمومکانیکی برینسون به همراه معادلات انتقال حرارت سیم‌های حافظه‌دار با معادلات غیرخطی تیر ترکیب شده و سیستم معادلات کوپله برای چند حالت خاص حل شده است. روش پیشنهادی در این مطالعه به آسانی قابل تعمیم به سازه‌های پیچیده که توسط سیم‌های حافظه‌دار، به صورت خارجی، تحریک می‌شوند، می‌باشد.

doi: *10.5829/idosi.ije.2012.25.03a.07*